

# Experimental Investigation on the Effect of Ring Tab on Mixing Enhancement of Subsonic Jets

K. Dhamodaran<sup>1</sup>, S. Thanigaiarasu<sup>2†</sup>, S. Venkatramanan<sup>1</sup>, R. Arun Prasad<sup>2</sup>, and M. Kaushik<sup>3</sup>

<sup>1</sup> Department of Aeronautical Engineering, KCG College of Technology, Chennai, Tamilnadu, 600097, India

<sup>2</sup> Department of Aerospace Engineering, MIT Campus, Anna University, Chennai 600044, India

<sup>3</sup> Department of Aerospace Engineering, Indian Institute of Technology, Kharagpur, West Bengal, 721 302, India

†Corresponding Author Email: [sthanigaiarasu@mitindia.edu](mailto:sthanigaiarasu@mitindia.edu)

## ABSTRACT

For thrust vectoring, combustion characteristics, infrared radiation reduction, and aeroacoustics noise mitigation, the mixing enhancement and core length reduction of a jet must occur without a substantial loss of thrust. Manipulating flow parameters enables the enhancement of the jet mixing process. Nozzle exits fitted with varying tab designs have the potential to alter the flow characteristics in the subsonic jets. The present study uses a ring tab to investigate the influence of the jet spread. These tab configurations are the source of creating counter-rotating vortices of varied sizes due to their even curvature in the plane of the flow. Non-uniform vortices at the orifice perimeter cause differential jet spread, resulting in axis switching and improved mass entrainment properties. The experimental results of the ring tab are compared with the free jet configuration at subsonic exit Mach numbers 0.4, 0.6 and 0.8. The Ring tab showed a significant decrease in the potential core, with reductions of 40%, 60% and 91.67% at Mach numbers 0.4, 0.6 and 0.8, respectively, indicating a substantial improvement in jet mixing. Additionally, the jet decay was faster than the free jet, demonstrating the potential of the ring tab in altering flow characteristics. The radial profiles and Mach contour plots illustrate the Mach decay, indicating the rate at which the jet spreads and the jet deflection from its centerline. This study presents a new tab configuration by providing a single circular ring tab instead of the typical dual tab layout. The main objective of this experimental study involving ring tab is to enhance jet mixing and perhaps decrease the core length, with potential applications in reducing noise and providing thrust vectoring in aircraft engine jets.

## Article History

Received November 21, 2024

Revised January 21, 2025

Accepted February 25, 2025

Available online May 5, 2025

## Keywords:

Mixing enhancement

Jet mixing

Jet deflection

Ring tab

Potential core reduction

Axis switching

Kelvin Helmholtz instability

## 1. INTRODUCTION

The improvement of jet mixing is a crucial factor in numerous engineering applications that include jet flows. The significance of jet mixing enhancement lies in its applications, including the reduction of noise in commercial aircraft, the decrease of thermal trace in combat jets, and the development of the efficiency of the combustion cycle. Consequently, it has been the subject of ongoing and thorough investigation for decades. Jet control can be categorized into two main strategies: active control and passive control. These techniques are used to improve the mixing of jet flows, depending on the specific applications and requirements. In the former, modifications such as vortex-generating devices (tabs), chevron patterns, grooves, or perforations are utilized at the nozzle output to induce flow disruptions. The

enhanced mixing diminishes the level of noise. The supersonic ejector enhances thrust by improving the interaction between the main and secondary fluids. Thrust direction is altered using an aerodynamic-based jet control technique, resulting in the advantageous application of thrust vectoring.

Jet control involves modifying the jet's mixing properties to enhance the system's performance. As the jet emerges from the nozzle, the swirling structures at the outer edge of the jet provide suction and assist in drawing in the surrounding fluid with relatively low momentum. Although large-scale structures are effective entrainers, their lifespan is shortened because their higher inertia causes them to break apart quickly into comparatively smaller, fine-scale structures. The intricate formations have a crucial function in facilitating the mixing of

**NOMENCLATURE**

D	diameter of the nozzle exit	X	distance along the axial direction of the jet
M	Mach Number	Y	distance along the radial (vertical) direction of the jet
M <sub>j</sub>	Mach Number at the nozzle exit	Z	distance along the radial (lateral) direction of the jet
P <sub>0</sub>	settling chamber pressure	γ	specific heat ratio
P <sub>atm</sub>	atmospheric pressure		

streams with the adjacent fluid. However, they do not contribute to mass entrainment (Crow & Champagne, 1971). By studying the processes of vortex creation, merging, and breakdown, one can gain control over the jets by comprehending the intricate topology of both large- and small-scale structures. Jet shear layer growth and entrainment are controlled by the evolution and breakup of the axisymmetric jet's azimuthal vortices (Brown & Roshko, 1974). Bradbury and Khadem (1975) conducted an experimental study to examine the impact of mechanical tabs on low-speed jets, which are small extensions at the exit of a nozzle. Their findings indicated that including tabs significantly increased the jet spread rate, reducing the potential core length and causing the jets to bifurcate. In a further investigation conducted by Ahuja and Brown (1989), it was found that the mechanical tabs used at various locations and numbers were equally efficient in enhancing the mixing of the jet at high velocities and reducing the noise produced by the jet. Ahuja (1990) discovered that the mechanical tabs attached at the nozzle outlet produce significant jet mixing, especially at subsonic speeds. Additionally, employing mechanical tabs at supersonic speed will reduce noise. Zaman et al. (1992), Samimy et al. (1993), and Zaman et al. (1994) conducted experimental research to examine the impact of mechanical tabs on distortion. The tabs generate a pair of vortices in the direction of the flow, which have been identified as the cause of the entrainment and substantial spreading of the jet.

In their experimental study, Behrouzi and McGuirk (1998) found that parameters such as the projected region, size, width, structure, and angle of alignment of a tab substantially impact jet decay. The findings indicated that higher tabs resulted in more significant jet degradation. In their trials, Dharmahinder Singh Chand et al (2011) discovered that the width of the tabs was more efficient in enhancing jet mixing than their length while having the same projected area. Experimental research on the geometrical impacts of fixing tabs at a convergent nozzle's exit plane under expanded sonic jet circumstances at various tab orientations was conducted by Thanigaiarasu et al. (2008). Compared to the other two configurations—arc-tab facing-out and rectangular tabs—the arrangement with arc-tab facing-in, which they employed at all blockage levels, proved more effective. The observed reduction in core length was 80% with the former arrangement and only 40% with the latter, which includes jets with rectangular tabs and an arc tab facing out. Bridges (2003) examines how mixing augmentation techniques can diminish jet noise. Experimental and analytical observations have shown that reducing the diameter of a jet and manipulating turbulence can effectively minimize jet noise. In a study by Lovaraju and Rathakrishnan

(2007), the researchers examined the comparative efficiency of subsonic and sonic axisymmetric jets regarding their cross-wire effectiveness. The jet mixing achieved was highly efficient immediately after exiting the nozzle, even when cross-wires were present at all Mach numbers.

In their experimental investigation, Ahmed et al. (2013, 2015, 2016), examined the effects of solid tabs (tabs without holes) and tabs with straight perforations and slanted perforations on the jet at various subsonic Mach values. The findings indicate that solid tabs have a greater impact in far downstream directions than perforated tabs. In addition, the diagonal perforation in tabs created streamwise vortices oriented towards the jet's centerline. This disrupted the potential core region of the primary jet, leading to a more rapid decay of the jet. Richards et al. (2023) investigated the effects of tabs with uneven projections on the formation of counter-rotating vortices. These vortices cause shear distortion and instability at the nozzle exit. These implications ultimately result in significant reductions in the core's length and the presence of asymmetrical decay characteristics with total pressure. Thanigaiarasu et al. (2023) investigated the potential use of vanes to enhance jet mixing properties and examined the influence of vane length and number on jet characteristics. Thanigaiarasu et al.'s (2020) study looks at how well circular solid tabs and circular tabs with holes work to improve the mixing of axisymmetric subsonic jets. Both solid circular tabs and circular tabs with holes have been seen to greatly improve the blending of jets. The possible core length was decreased by 37.5% and 62.5% for the circular tab with perforation and solid tabbed jet, respectively, compared to the free jet. It is also evident from Lovaraju and Rathakrishnan (2006) that the thrust loss is directly proportional to the blockage caused due to fitment of tab at the nozzle exit. Various literatures also suggests that the maximum blockage ratio of 10% is used in enhancing the jet mixing.

Jyothy et al. (2023) revealed that the wedge-shaped jet tabs thrust vector control system (TVC) could achieve a thrust deflection angle of 4.14° by utilizing a variety of wedge thickness and height combinations in different operational conditions. The results indicate that this TVC system has substantial potential as replacement for secondary injection methods, as it eliminates the necessity for a fluid reservoir. Richards et al. (2024) conducted an investigation into the innovative vortex generator tab, which is asymmetrically located and promotes mixing. The researchers found that the vortex generator obtained a potential core reduction of approximately 85% for the correctly expanded sonic jet and 77% for Mach 0.8 and 0.6 jets, respectively.

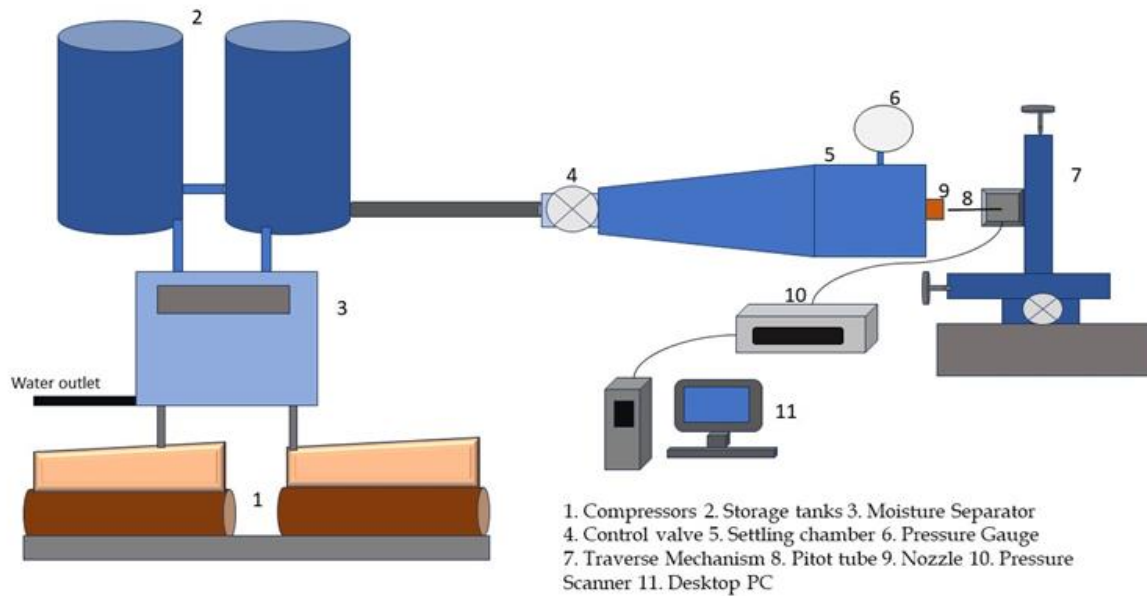


**Fig. 1. Schematic layout of the experimental jet facility**

The experiments conducted by [Tong and Warhaft, \(1994\)](#), [Sadeghi & Pollard \(2012\)](#), and [Parker et al. \(2003\)](#) involved inserting a thin passive ring symmetrically into the mixing layer of a circular jet near the nozzle outlet. The results showed that introducing a ring in the mixing layer decreased the mixing layer's growth rate and the jet's spread rate. The predominant focus of jet control research has been on using pairs of rectangular or delta shapes, both with and without perforation, as well as corrugated topologies of vortex generators, to manipulate flow. A few studies have been done on the passive ring arrangement of vortex generators to change the rate of jet spread and the formation of mixing layers.

In this research, rather than a pair of tabs, a single circular ring tab is utilized to assess the possible core variation and spread rate, comparing both with a free jet. To find out how better mixing works and how the jet grows at subsonic Mach numbers of 0.4, 0.6, and 0.8, a full experimental study was carried out using a circular ring tab placed at the exit of a convergent nozzle. The subsequent section comprehensively explains the tab's dimensions and blockage region at the nozzle flow region.

## 2. EXPERIMENTAL METHODOLOGY

### 2.1 Experimental Jet Facility

An experiment was conducted at the high-speed jet facility at KCG College of Technology in Chennai. A jet facility consists of air compressors, two storage tanks, a settling chamber, an air drier unit, a pressure gauge, a control valve, a traverse mechanism, and a pressure scanner with a pitot tube. The diagram illustrating the arrangement of the experimental jet facility layout is depicted in Fig.1. A dual-phase, three-cylinder piston compressor was utilized to compress the surrounding air, which was subsequently held in two sizable storage tanks, each with a capacity of 4000 liters. The highest storage pressure capacity is 25 bar. Following compression, the air is directed to

dedicated air dryer equipment, where all moisture is extracted before being stored in the tank. The compressed air is directed through a gate valve and control valve before being released into a settling chamber. The settling chamber has mesh screens to minimize turbulence and ensure a smooth flow as the air enters the nozzle. A pressure gauge is installed in the settling chamber to regulate the pressure, enabling expansion in the nozzle. The test nozzle models are affixed to the outflow flange via a threaded connection. Adjusting the pressure regulator during a run can change the settling chamber pressure. The stagnation pressure level determines the settling chamber's different nozzle pressure ratios (NPR). The nozzle pressure ratio (NPR) refers to the stagnation pressure ratio to ambient or back pressure. The settling chamber maintains an ambient temperature. The pressure transducer gauged the pressure within the settling chamber for each iteration. A photograph illustrating the indoor sections of experimental jet facility is presented in Fig.2 and 3., which showcases the instrumentation used.

### 2.2 Instrumentation

#### 2.2.1 Traverse Mechanism

This study employed a 3D traverse mechanism to place the pitot tube and detect the pressure in the flow emanating from the nozzle. The device is equipped with a stepper motor and utilizes specialized software to accurately control the movement of the spindle along the X, Y, and Z axes. The traverse mechanism had a linear resolution of approximately 0.1 mm, while the probe's positioning accuracy was  $\pm 0.1$  mm. The Pitot tube, affixed to the traversing mechanism shown in Fig. 3, could traverse up to 600 mm in the three directions.

#### 2.2.2 Pitot Pressure Probe

The pressure was measured using a Pitot probe on a 3-D traverse system. The probe was aligned to directly intersect the jet stream emanating from the nozzle exit. A Pitot probe is a cylindrical tube with a rounded,

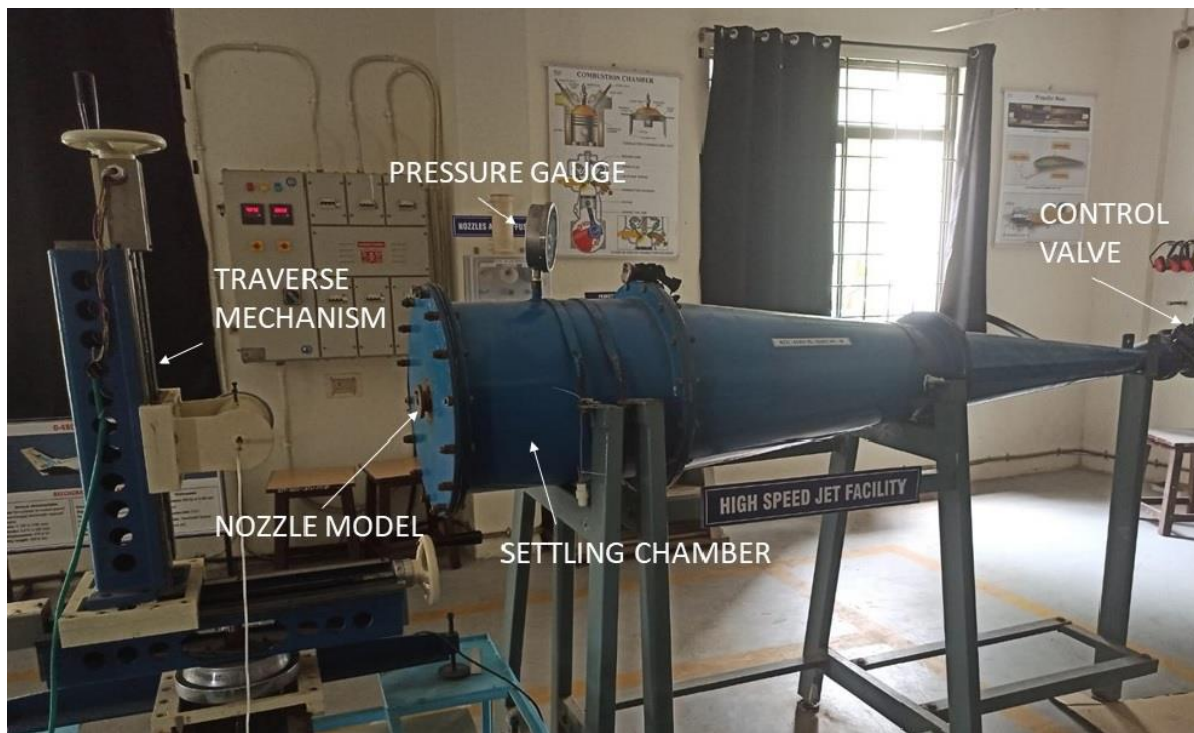


**Fig. 2** Photographic view of the indoor sections of the experimental jet facility

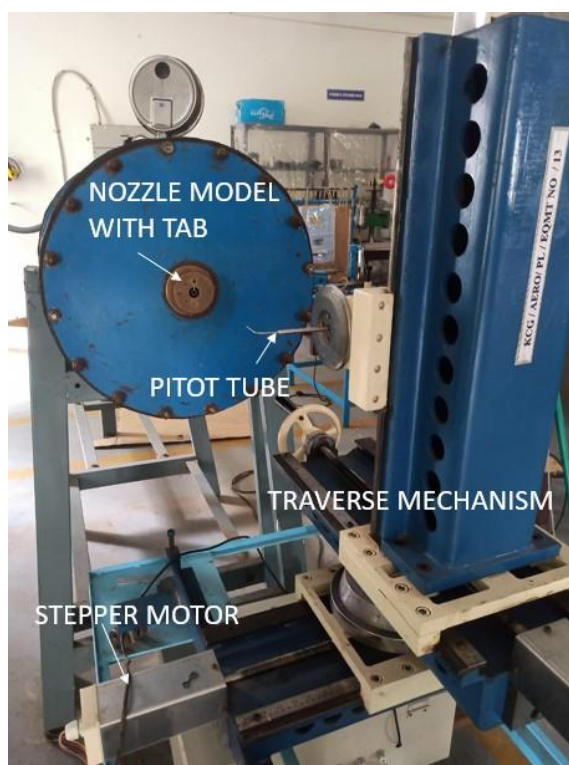


**Fig. 3** Photographic view of the jet facility with nozzle model and pitot tube

unsharpened tip that is oriented towards the motion of the air stream. The Pitot probe possesses an internal diameter of 0.4 mm and an outside diameter of 0.6 mm. The pitot probe area to nozzle exit area ratio is  $0.9 \times 10^{-3}$ , which falls below the optimum value of  $15 \times 10^{-3}$ . Furthermore, due to the high Reynolds number of the jet Mach numbers examined in this study, the influence of viscosity on the

pressure readings is considered insignificant. The pitot probe is perpendicular to the flow, with the measuring port directed towards the flow. Considering the isentropic flow events, the measured pitot pressure is converted to an equivalent flow Mach number.

### 2.2.3 Pressure Scanner

Pressure measurements are taken using a 16-channel pressure transducer. A Pitot probe is connected to the transducer to monitor the pressure in the jet field. The transducer can accurately measure pressures between 0 and 20 bar with a precision of  $\pm 0.15$  of the maximum measurement range. The device can gather 300 pressure readings per second to calculate the typical pressure value.

### 2.3 Tab Model

The experiment utilized a convergent nozzle with an inlet diameter of 40 mm and an exit diameter of 20 mm. The nozzle features a threaded design at one end, securely attaching it to the settling chamber flange. The object was constructed from brass, measuring a total length of 50 mm and featuring a convergence angle of 11.3 degrees. This study utilized a passive jet control approach. Instead of employing a pair of tabs at the exit of the nozzle, a solitary tab with a circular configuration made out of mild steel is utilized. The study used a circular ring with an outside circle diameter of 10 mm, an inner circle diameter of 9mm, and a thickness of 0.5 mm. A rectangular strut is employed to secure the ring at the central position of the nozzle's exit on one side. In contrast, the other side is used to fasten the tab with a screw onto the nozzle, as shown in Fig. 4. A projected strut dimensions are 5 mm in length along the tab from the nozzle exit circle boundary and a width of 1.5 mm to hold the ring. Due to a strut at one end, this tab provides the asymmetric projections. To avoid a decrease in thrust, the blockage ratio of tabs should be maintained



**Fig. 4** Photographic view of the circular ring tab mounted at the nozzle exit

at 10% of the nozzle exit area. Hence, the circular ring tab is specifically constructed with a total area of 14.93 mm<sup>2</sup> and a projected strut area of 7.5 mm<sup>2</sup> in the flow. Therefore, the total size of the tab is 22.43 mm<sup>2</sup>, which is smaller than the blocking area of 30 mm<sup>2</sup>, to prevent any loss of thrust. The ring tab is specifically engineered to have no angular edges except for the areas where the struts secure the ring. The blockage ratio of the ring tab is 7.14% which is lesser than 10% of allowable blockage ratio from the previous literature. A schematic diagram of the tab arrangement on the nozzle and an isometric view of the ring tab is shown in Fig. 5.

When flow passes through a nozzle exit, uniform vortices are created around its perimeter. Uniform vortices in and around the circular ring tab additionally generate transverse vortices. The presence of a strut causes transverse vortices to form along both sides, which then turn into streamwise vortices starting from the edge of the strut and extending outward. A similar methodology of creating streamwise vortices from rectangular tabs were discussed by Venkatramanan et al. (2024). The stagnation

points exert force on the circle of the ring and strut surfaces exposed to the flow, creating a low-pressure area on the opposite side of both surfaces. Therefore,  $dP/dr$  is evaluated in the radial direction of the ring, whereas  $dP/dy$  is assessed in the strut direction, as shown in Fig.6. Therefore, in the present investigation, vortices created from the ring tab has two components. One set of vortices are created at the edges of the strut throughout its length similar vortices generated from rectangular tabs. The other components of the vortices are created from the inner and outer edges of the ring surface. Therefore, vortices created from both strut and ring surfaces travel downstream and increases the jet mixing.

Jet flow occurs within the central ring core and surrounding the ring tabs. This can be regarded as the primary flow passing through the ring and the secondary flow occurring adjacent to the ring, generating shear forces between the flows. Schematic diagrams illustrating azimuthal vortices shed from the ring tab, as shown in Fig. 6. Additional examinations of the tab will be covered in the discussion section.

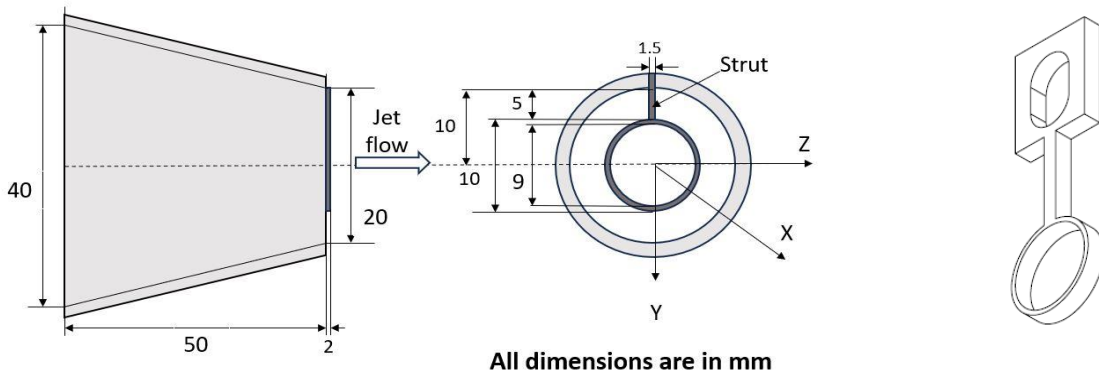
### 2.4 Test Conditions

This study investigates the ring tab's impact on mixing efficiency in subsonic flow conditions. Additionally, a free jet was tested for comparison purposes. Adjusting the pressure in the settling chamber can achieve the desired nozzle exit Mach number, which can be calculated by applying the isentropic relation to the Nozzle Pressure Ratio (NPR).

$$\frac{P_0}{P_{atm}} = \left(1 + \frac{\gamma-1}{2} M^2\right)^{\frac{\gamma}{\gamma-1}} = NPR \quad (1)$$

$$M = \sqrt{\frac{2}{\gamma-1} \left[ \left(\frac{P_0}{P_{atm}}\right)^{\frac{\gamma-1}{\gamma}} - 1 \right]} \quad (2)$$

Where subscripts 0 and atm denote stagnation and local atmospheric conditions, respectively;  $P_0$  refers to the settling chamber pressure;  $P_{atm}$  refers to the atmospheric pressure;  $\gamma$  is the ratio of specific heats, which is equal to 1.4 for air; and  $M$  is the Mach number of the nozzle exit at different axial locations in the flow field.



(a)

(b)

**Fig. 5** Schematic diagram of (a) convergent nozzle with tab and (b) isometric view of ring tab

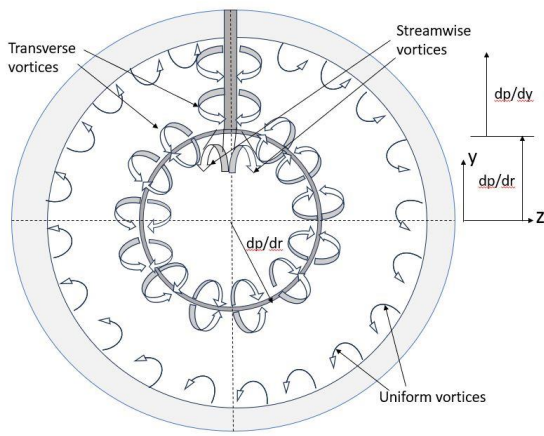


**Fig. 6 Schematic diagram of vortices shed from a circular ring tab**

Pressure measurements were conducted in streamwise directions to assess the potential reduction in the possible core length. The extent of the jet dispersion was measured by analyzing the pressure data collected in the radial directions. Pressure measurements were taken at jet Mach numbers of 0.4, 0.6, and 0.8. The equations 1 & 2 generate plots along three axes, which will be further elaborated upon in the following section.

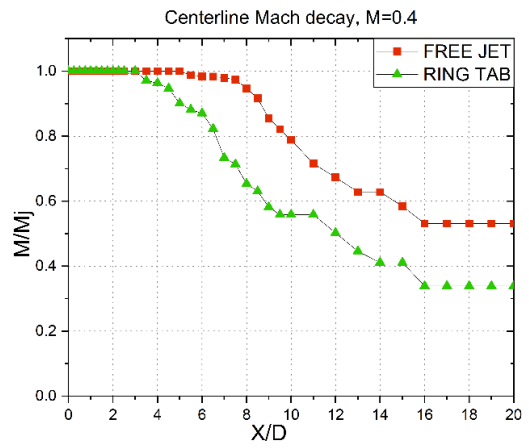
### 3. RESULTS AND DISCUSSION

All locations are nondimensionalized along three axes by utilizing the nozzle discharge diameter. The jet axis is the line emanating from the nozzle outlet's center and extending downstream. The axial coordinates along the jet's axis are denoted by  $X/D$ , a ratio of the axial length to the diameter of the nozzle exit. In the tab direction, the radial locations are denoted by  $Y/D$ , which is the ratio of the radial distance between the jet axis and the exit of the nozzle diameter. In the same way, the radial positions perpendicular to the tab are denoted by the ratio  $Z/D$  as measured along the flow axis. The Mach number ( $M$ ) measured at any place is normalized using the nozzle jet Mach number ( $M_j$ ). The Mach number at any given place is denoted as  $M/M_j$ .

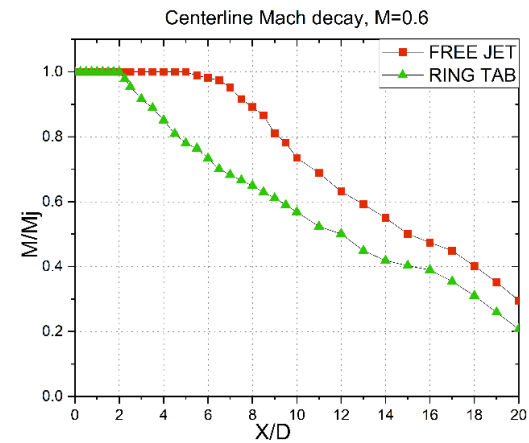
#### 3.1 Centerline Mach Decay

The decay of a jet can be detected by observing a decrease in the length of the potential core along the centerline of the nozzle. This can be accomplished by implementing a tab at the exit of the nozzle. The tab induces a pair of streamwise vortices that facilitate mixing the surrounding fluid with the jet fluid by interacting with the shear layer. This research employs a singular tab as a ring-like structure instead of a pair of rectangular or triangular tabs. The dimensions of tabs were previously described in the methods section. A velocity decay comparison is conducted between a free jet and a ring tab-controlled jet at Mach numbers of 0.4, 0.6, and 0.8, as illustrated in Fig.7 (a) - (c)

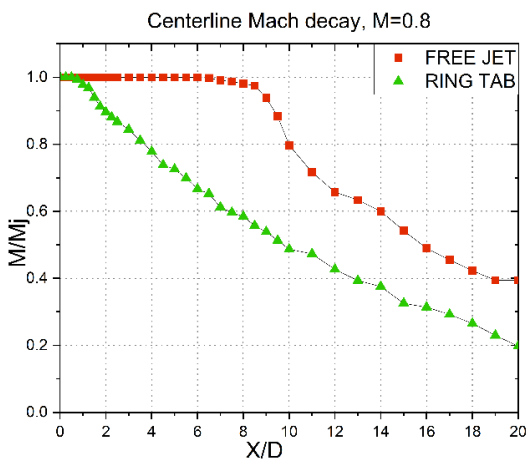
In the context of the ring tab, no angular edges were observed along the circular ring, except for the interface where the strut encounters the ring. Hence, the jet's



(a)  $M = 0.4$



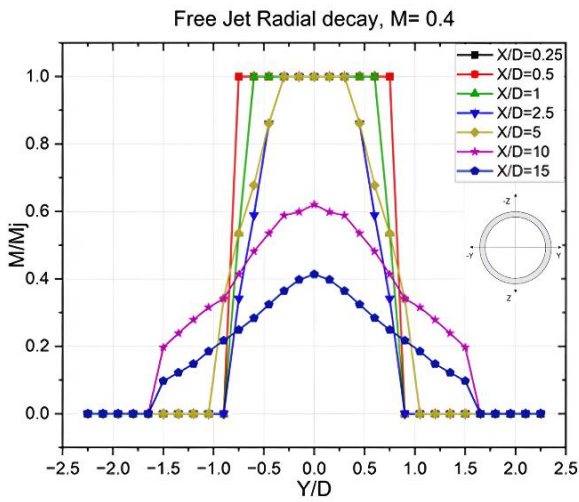
(b)  $M = 0.6$



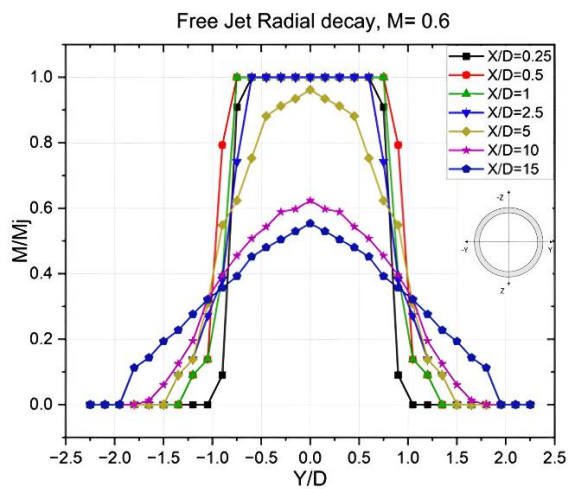
(c)  $M = 0.8$

**Fig. 7(a)-(c). Centerline Mach decay for free jet and ring tab-controlled jets at different Mach numbers**

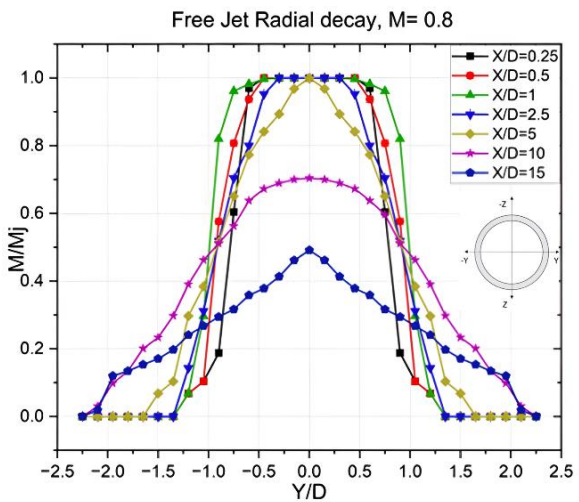
redirection occurs within and near the circular areas of the ring tab. In the context of co-flow, the primary flow of the jet is considered to happen inside the ring, while the secondary flow occurs around the outside ring. This configuration facilitates shear layer contact between the primary jet and secondary jet, as well as between the secondary jet and the jet boundary of the nozzle exit.



(a)  $M = 0.4$



(b)  $M = 0.6$



(c)  $M = 0.8$

**Fig. 8 (a)-(c). Mach decay profiles for the uncontrolled jet in the radial direction at different Mach numbers**

The level of mixing significantly rises as the Mach number increases, as the presence of shear layers leads to the formation of streamwise vortical rings in the flow

field, resulting in contact between different layers. The experiment was conducted in a subsonic environment, allowing for the conversion of the recorded pitot value to a Mach value. This conversion is based on the atmospheric pressure at the point of jet discharge, which is the static pressure because of the proper expansion of subsonic jets.

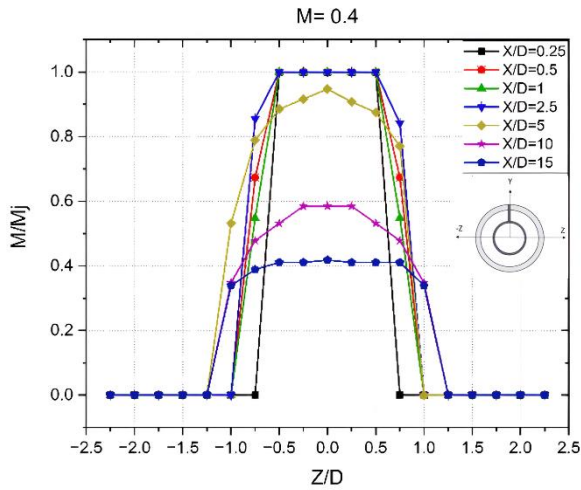
At a Mach number of 0.4, the potential core length (PCL) of the ring tab is reduced from 5D to 3D, as compared with the free jet, as illustrated in Fig. 7(a) - (c). At a Mach number of 0.6, the PCL of the ring tab is decreased from 5D to 2D. At a higher subsonic Mach number of 0.8, the PCL decreases significantly from 6D to 0.5D. The velocity decay starts from 3D and reaches a fully developed zone at 11D for  $M = 0.4$  of the ring tab jet, as seen in Fig. 7(a). Compared to the free jet, the ring tab significantly reduces the core length by mitigating the Kelvin Helmholtz instability within and around the flow of the ring and nozzle jet boundary. The circular ring tab facilitates the development of large-scale coherent structures, resulting in a significant decrease of core length around 40%, 60%, and 91.67% at Mach numbers 0.4, 0.6, and 0.8, respectively. Also, the velocity decay characteristics of the ring tab-controlled jet are higher than the free jet.

### 3.2 Radial Decay Plot Z/D (Normal to the Tab direction)

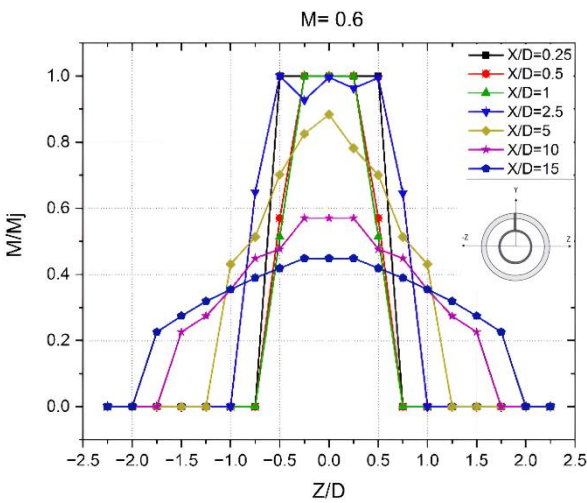
To determine the radial decay of the free jet and tab-controlled jet at various axial locations, it is essential to consider the nondimensionalised Mach ratio, similar to how it is done for the centerline plot. Figure 8 & 9 display the radial decay profile of the Mach number in the radial direction for the free jet and ring tab at Mach numbers of 0.4, 0.6, and 0.8 in the Z and Y directions, respectively.

The velocity depicts a top hat profile at axial location of near-field and intermediate regions, specifically at  $X/D = 0.25, 0.5, 1$  and  $2.5$  as illustrated in Fig. 8 (a), and remains constant in the radial direction at a Mach number of 0.4. The velocity of the jet starts decreasing substantially from the top hat profile along the jet's axis at  $Y/D = 0.5$  to  $-0.5$  at an axial distance of  $X/D = 1$  similar to the trend noticed by Jebaz et al. (2023). The jet begins to merge with the ambient fluid at the intermediate area of  $X/D = 5$ , resulting in a decrease in radial velocity. The characteristic velocity of the jet is reduced as indicated by the decrease in  $M/M_j$  to 0.6 and 0.4 at  $X/D = 10$  and 15, respectively as depicted in the Fig. 8(b) and 8(c). Comparable outcomes were observed at Mach numbers of 0.6 and 0.8; however, the velocity at which the jet spreads downstream escalated with an increase in Mach number. In the context of the ring tab, the velocity decay, with a value of  $M = 0.4$ , initiates at a position  $X/D = 5$  due to the vortex shedding, which causes the surrounding fluid to enter the jet. At  $X/D = 10$  and 15, there is a region where the velocity remains constant across the axis, and there is a decrease in elevation at  $Z/D = 1.5$  shown in the Fig. 9 (a).

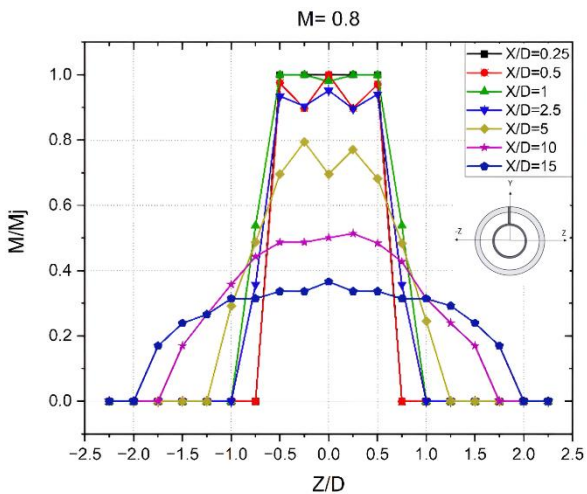
Figure 9(b) shows Jet bifurcation with three peak velocities of  $M/M_j = 1$  at  $X/D = 2.5$  for Mach number 0.6. The reduction in peak velocity value of  $M/M_j$  is 0.75, 0.58, and 0.44 for  $X/D$  locations of 5, 10, and 15, respectively.



(a)  $M = 0.4$



(b)  $M = 0.6$



(c)  $M = 0.8$

**Fig. 9(a)-(c) Mach decay profiles for the ring tab-controlled jet at different Mach numbers along the Z-axis (normal to tab)**

By observing Fig. 9(c), it can be shown that the maximum peak velocity of  $M/M_j$  is 0.8, 0.5 & 0.35 is found at  $X/D = 5, 10$  &  $15$ , respectively, for  $M = 0.8$  as compared with the free jet. Figure 9(c) illustrates the jet

bifurcation by forming W-shaped and M-shaped profiles at axial locations of 0.5, 1, and 2.5. This is caused by the shedding of vortices from the ring tab, resulting in velocity variations and fluid engulfment. Furthermore, jets are extensively distributed up to  $Z/D = 2$  to  $-2$  at Mach numbers of 0.6 and 0.8, displaying similar characteristics at positions  $X/D = 10$  and  $15$ . The tab-induced vortex facilitates the bulk transfer of ambient fluid into the jet, resulting in superior mixing to the free jet. At a Mach number of 0.4,  $M/M_j$  is 0.6 at  $X/D = 16$ . This demonstrates the delay in decay induced by the rise in momentum of these vortices at low subsonic Mach numbers. When comparing with the free jet, a little discrepancy results in the near field and intermediate region due to the variation in vortical structures. Additionally, the jet spreads widely at that location due to the assimilation of surrounding fluid mass into the jet flow field.

### 3.3. Radial decay Plot $Y/D$ (Along the Tab direction)

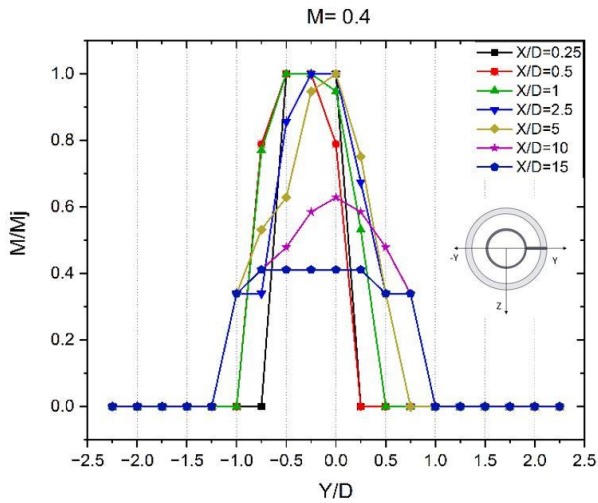
When the jet passes by the strut on one side of the tab, it experiences a substantial alteration in its direction, regarded as the positive direction. There is no apparent strut arrangement on the negative side of the  $Y$ -axis. This allows the jet to flow freely without deviation, indicating asymmetric flow in the flow field. Figure 10(a)-(c) displays the  $Y/D$  radial decay plot for the ring tab. The maximum velocity of  $M/M_j = 1$  is shifted from the origin to a position  $0.25D$  along the negative  $Y$ -axis at  $X/D = 2.5$ , with a Mach number of 0.4, due to the asymmetric projection depicted in Fig 10(a). At a  $Y/D$  value of

$-0.5$ , the peak velocity of  $M/M_j$  is 0.63 & 0.45, and the values of  $M/M_j$  are 0.62 & 0.43 at  $M$  values of 0.6 and 0.8, respectively.

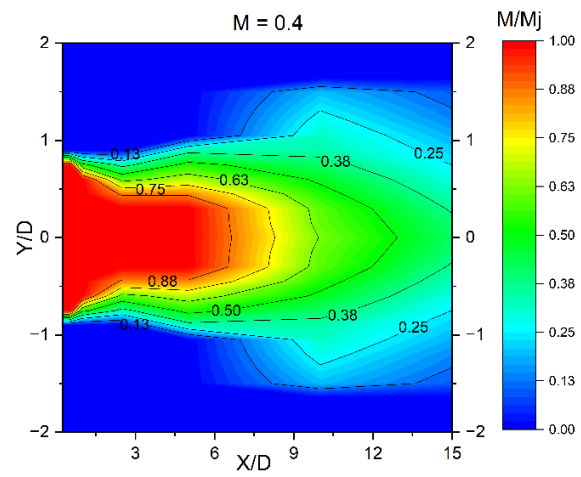
The velocity variations are more pronounced in the near-field and far-field regions, which causes a change in direction in the  $Y$ -plane. The flow axis underwent shifting at various speeds across distinct axial locations. Compared to the  $Z$ -axis, the dispersion of the jet is much reduced in the near field. This is mostly caused by the shedding of large-scale vortices from the strut, leading to a substantial mass concentration on one side of the jet flow. The jet spread was observed from the  $Y/D$  radial plot in the Fig.10(a)-(c) shows significant jet deflection from the centerline of the jet. For  $M = 0.4$ , the maximum peak velocity was observed at  $Y/D = -0.25$ , causing the jet to deflect from the centerline at an angle of  $1.4^\circ$ . Meanwhile, for  $M = 0.6$  and  $0.8$ , the maximum peak velocity was observed at  $Y/D = -0.5$ , indicating that the jet was deflected by an angle of  $2.9^\circ$ .

Therefore, jet deflection is achieved by asymmetrically placing a strut in a ring tab configuration generated by the strut and its interaction with the boundary layer of the jet. Consequently, effective blending occurs when the mass in the flow field increases when the ring tab is used. The radial plot of the  $XZ$  plane indicates that the tab-controlled jet has a greater jet spread than the free jet because of the transverse vortices created around the ring tab, which entrain more of the surrounding fluid.

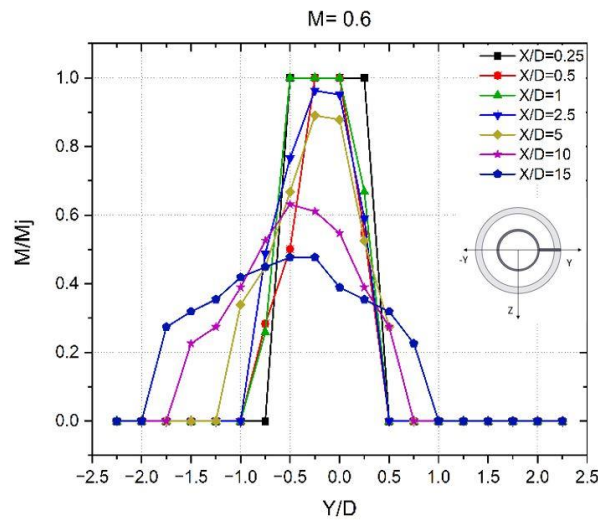
Hence, the plot's data demonstrates axis-switching phenomena on the ring tab along the  $Y$ -axis.



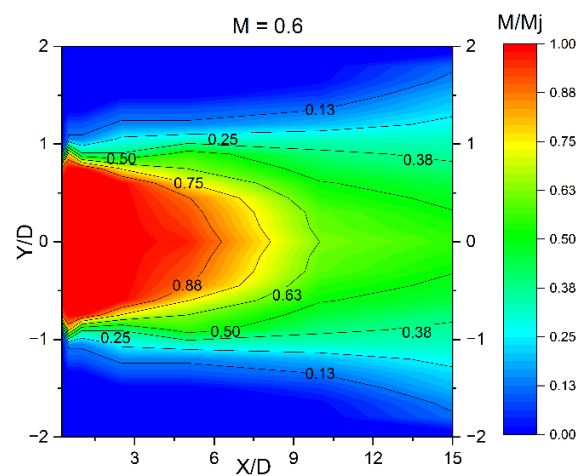
(a)  $M = 0.4$



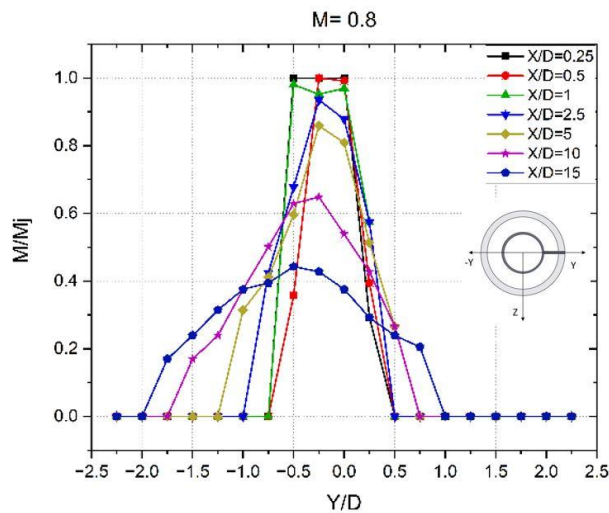
(a)  $M = 0.4$



(b)  $M = 0.6$

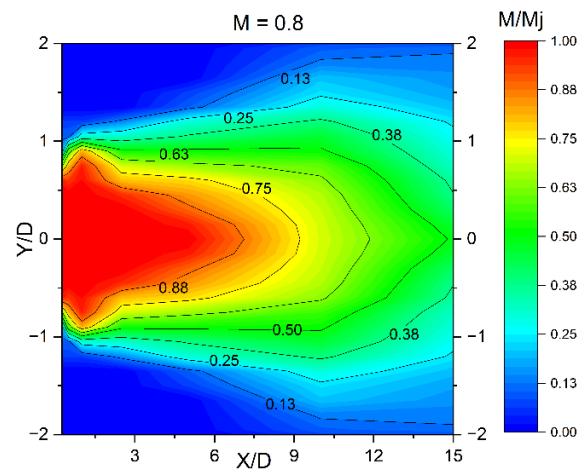


(b)  $M = 0.6$



(c)  $M = 0.8$

**Fig. 10(a)-(c) Mach decay profiles for the ring tab-controlled jet at different Mach numbers along the Y-axis (along the tab)**



(c)  $M = 0.8$

**Fig. 11(a)-(c) Mach Contour profile for free jet condition at different Mach number**

### 3.4. Mach Contour Plot in XZ Plane

Mach Contour plots were generated using experimental data for the free jet and ring tab along the XY & XZ plane, as shown in Fig. 11 & 12, respectively.

A jet spread refers to a mass movement in the flow field caused by the formation of massive vortices on the boundary layer. For Mach numbers 0.6 and 0.8, the jet spread widely in the  $Y/D$  location of 2.0 to -2.0, as seen in Fig. 11(b) & (c).

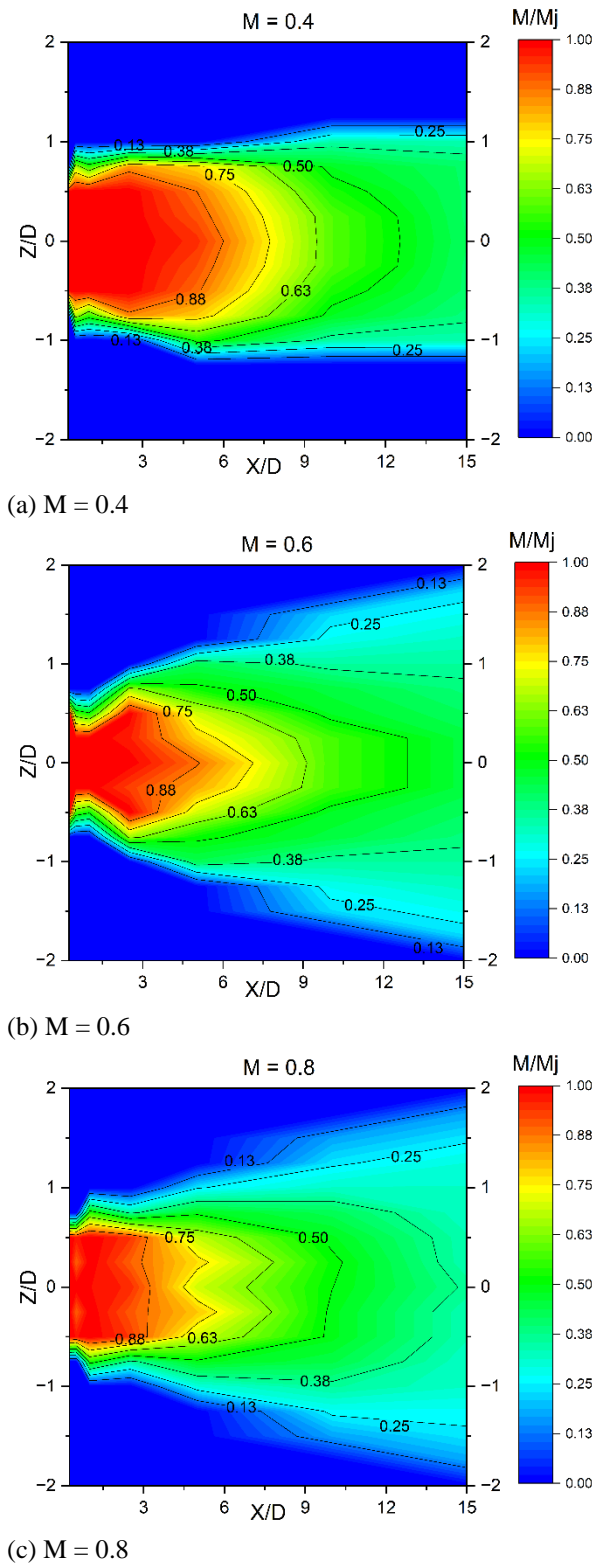


**Fig. 12(a)-(c) Mach Contour profile for ring tab-controlled jet at different Mach numbers along the Z-axis (normal to tab)**

Figures 12(b) and (c) illustrate the substantial spread of the ring tab jet, achieving up to a ratio of  $Z/D = 1.6$  at Mach numbers of 0.6 and 0.8. This observation demonstrates the presence of the fluid mass around the intermediate region flow field at  $X/D = 6$  to  $X/D = 9$  and its increase in the downstream region. In the ring tab, the

expansion of the jet widens as the Mach number increases and the possible core length decreases.

The central core of the free jet is larger than the jet of the ring tab. However, the jet spread is smaller than that of the jet-controlled tab, resulting in more mixing in the flow. Additionally, the plot shows a reduction in the asymmetrical flow caused by the vortices generated by the strut and their interaction with the boundary layer of the jet. As a result, the ring tab is employed to achieve effective integration by increasing the mass in the flow field.

### 3.5 Mach Contour Plot in XY Plane

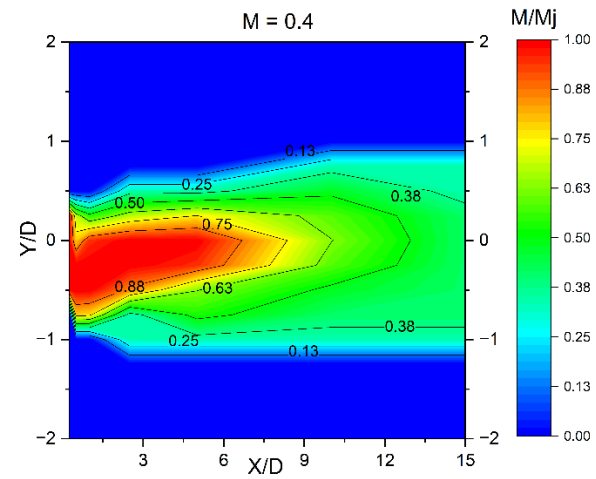
Similar to the preceding section, the contour plots displayed in Fig.13. are for the XY plane. The jet deflection occurs in the near-field region for tab-controlled jet flows due to a strut on one side of the ring tab. At lower velocities, the jet's potential core deflection in the near field region is mostly influenced by the pressure differential, as depicted in Fig.13(a). The dispersion of the jet occurs uniformly in the distant field area. At  $M = 0.6$ , the velocity ratio of  $M/M_j = 0.13$  attained at  $Y/D = 0.8$  in the positive direction and  $Y/D = -1.8$  in the downward direction at  $X/D = 15$  is seen in Fig 13(b). For the Mach number of 0.6 and 0.8, the Jet spread is deflected along the  $Y/D$  location from 0.75 to -1.75 and 1 to -2 at  $X/D = 10$  & 15, respectively, with peak velocity shifted to  $Y/D = -0.5$  is shown in Fig 13 (b) & (c). The jet deflection is seen in the downstream section of the flow, which indicates the asymmetric flow and axis shifting in this plane. The evident reduction in the potential core is observed in this case, as opposed to the XZ plane.

The pair of streamwise vortices generated by the strut is the primary cause of the reduction in the potential core. When the velocity increases, the jet's deflection in the far field region is mostly caused by momentum combined with streamwise vortices released from the strut. Due to bigger eddies created by the strut, ambient fluid has higher entrainment on the upper side of the tab. This fluid carries more kinetic energy, which deflects the jet flow downward. However, ring tabs played a role in reducing the core size and increasing the spread of the jet. This indicates that mixing occurs largely due to the vortices generated from the corners of the tab's strut at higher subsonic Mach numbers. Hence, the plot's data demonstrates axis-switching phenomena on the circular ring tab along the Y-axis.

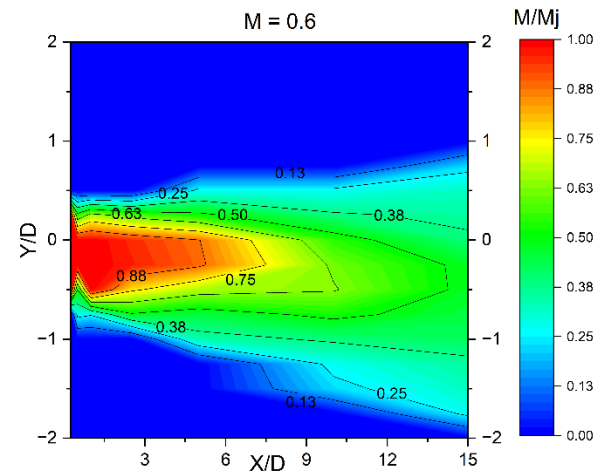
Additionally, this observation illustrates the deflection of the fluid mass in the vicinity of the flow field and its subsequent increase in the downstream region. As the Mach number increases and the potential core decreases, the flow in the ring tab widens on the negative side of the Y-axis. Furthermore, the strut's vortices induce as asymmetrical flow along the axial direction, as illustrated in the Fig 13 (b) and 13 (c).

### 3.6 Comparison of ring tab with conventional rectangular solid tab

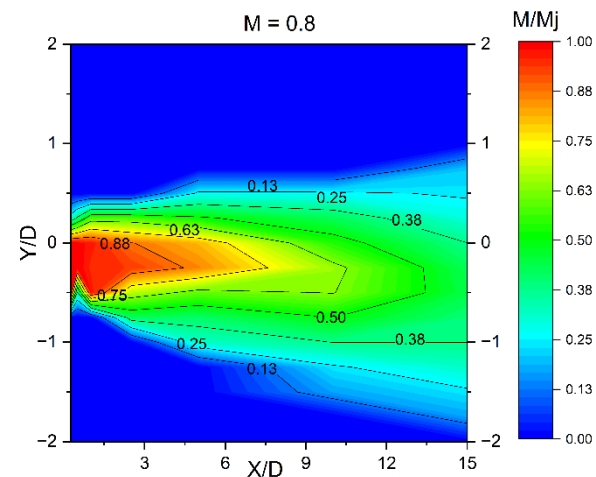
The comparison of jet characteristics for free jet, single ring tab and a pair of the conventional rectangular solid tab is carried out in axial and radial directions for nozzle



(a)  $M = 0.4$



(b)  $M = 0.6$



(c)  $M = 0.8$

**Fig. 13(a)-(c) Mach Contour profile for ring tab-controlled jet at different Mach numbers along the Y-axis (normal to tab)**

exit Mach number 0.6. A pair of rectangular solid tabs are positioned diametrically opposite each other at the nozzle exit. From the centerline Mach decay shown in Fig.14, the single ring tab and pair of solid tabs offer potential core decay of 60% and 45% respectively. From the decay curves it is also observed that ring tab and solid tab offers faster decay rates of 2 and 1.5 times more than the decay

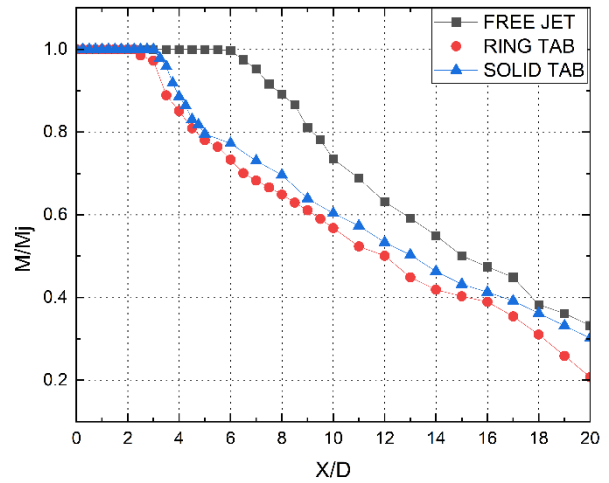


**Fig. 14 Comparison of centerline Mach decay profiles of Free jet, ring tab and solid tab at  $M = 0.6$**

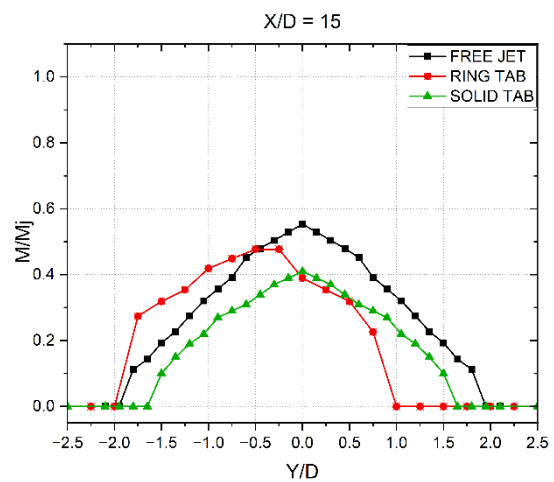


**Fig. 15 Comparative Mach decay profile for the ring tab and solid tab at  $M = 0.6$  along the Y-axis (along the tab)**

of free jet. In addition to vortices generated from the strut the ring tab creates additional vortices from inner and outer edges of the ring surface as in the Fig. Therefore it is evident that vortices created from the ring tab supported by the strut is more effective in the jet mixing than the conventional solid tab.

As illustrated in radial Mach decay shown in the Fig.15 for  $X/D = 15$ , the entrainment of ambient mass is greater on the negative side of the ring tab in the Y-direction. This is due to the large number of vortices that are generated from the periphery of the ring tab, which engulf the surrounding air into the jet flow. The peak velocity of  $M/M_j$  is offset from the jet's centerline by a distance of  $Y/D = -0.5$ . It is evident that flow deflection occurs in the downward direction for the ring tab as observed in the Fig.15, and the deflection is not observed in the conventional solid tab. Therefore the ring tab offers thrust vectoring capabilities along with superior mixing characteristics.

### 3.7 Applications and Scope of the Study

The outcomes of this study are significant as they demonstrate the potential core reduction and improved

mixing of the jet using a ring tab. A noteworthy discovery is that including a strut on one side of the ring tab causes the jet flow via the nozzle to migrate away from the centerline. By offsetting the ring tab away from the centre, a significantly greater amount of deflection becomes apparent. Regarding thrust vectoring applications, this special quality has important real-world effects on the aerospace sector. Furthermore, it is imperative to optimize the combustion efficiency of gas turbine engines and exhaust systems, as well as to mitigate noise and infrared signature emissions, by attaining faster mixing and dispersion of the tab-controlled jet. A future study may investigate the potential of adopting non-circular ring forms, such as the square, pentagon, and hexagon and also offset the ring tab from the flow axis of the nozzle.

#### 4. CONCLUSION

This study explores the impact of circular ring tabs on enhancing mixing and reducing the central core in subsonic jet flow regimes, particularly under free jet conditions. At a Mach number of 0.8, the potential core reduction of the ring tab is around 91.67%, which is much larger than the circumstances with Mach numbers of 0.4 and 0.6. This information indicates that the mixing intensifies as the jet's Mach number increases. By examining the radial plot, it is evident that the spread rate increases in the downstream direction as the Mach number increases for the ring tab. However, there is little fluctuation in the nearfield and intermediate regions due to the generation of vortices. The Mach contour charts illustrate the increased dispersion and deviation of the jet from the centerline caused by the strut of the tab. However, this study recognises the constraints regarding the blockage ratio that results in thrust loss. It emphasises the significance of designing the ring tab to optimise thrust for thrust vectoring operations. This tab configurations could vary the thrust vectoring capabilities of the jet and can be further investigated to measure the jet mixing abilities. This approach can boost mixing capabilities and reduce noise, increasing aircraft performance.

#### ACKNOWLEDGEMENTS

The authors sincerely thank Mr. Yadav, who worked on the circular solid tab, which provides insights into generating the ring tab for our study.

#### CONFLICT OF INTEREST

The author(s) have disclosed no conflicts of interest regarding the study's findings, creation, and dissemination of this paper.

#### AUTHORS CONTRIBUTION

**K. Dhamodaran:** Methodology; Formal analysis, Data curation; Writing -Original draft; **S. Thanigaiarasu:** Formal analysis; Writing - Review & Editing; Visualization; Supervision; **S. Venkatramanan:** Experimental Equipment/Venue; Writing – review &

editing; **R. Arun Prasad:** Resources and **M. Kaushik:** Investigation; Validation.

#### REFERENCES

- Ahmed, A. A., Thanigaiarasu, S., Venkatraman, S., Srinivasan, E., & Rathakrishnan, E. (2015). *Study of slanted perforated shapes in tabs for control of subsonic Jets*. 33rd AIAA Applied Aerodynamics Conference. <https://doi.org/10.2514/6.2015-2423>
- Ahmed, R. A., Thanigaiarasu, S., Kannah, D. L. V. V., Elangovan, S., & Rathakrishnan, E. (2016). Effect of Slanted Perforation in Tabs for Subsonic and Transonic Jets. *Fluid Mechanics and Fluid Power – Contemporary Research*, 795–809. [https://doi.org/10.1007/978-81-322-2743-4\\_75](https://doi.org/10.1007/978-81-322-2743-4_75)
- Ahmed, R. A., Thanigaiarasu, S., Santhosh, J., Elangovan, S., & Rathakrishnan, E. (2013). Study of slanted perforated jets. *International Journal of Turbo and Jet Engines*, 30(4). <https://doi.org/10.1515/tjj-2013-0015>
- Ahuja, K. (1990). An evaluation of various concepts of reducing supersonic jet noise. AIAA, 1990-3982. <https://doi.org/10.2514/6.1990-3982>
- Ahuja, K. K., & Brown W. H. (1989). Shear flow control by mechanical tabs. AIAA, 89, 0994. <https://doi.org/10.2514/6.1989-994>
- Behrouzi, P., & Mcguirk, J. J. (1998). Experimental studies of tab geometry effects on mixing enhancement of an axisymmetric jet. *JSME International Journal, Series B: Fluids and Thermal Engineering*, 41(4), 908-917. <https://doi.org/10.1299/jsmeb.41.908>
- Bradbury, L. J. S., & Khadem, A. H. (1975). The distortion of a jet by tabs. *Journal of Fluid Mechanics*, 70(4), 801-813. <https://doi.org/10.1017/S0022112075002352>
- Bridges, J. (2003). Control of jet noise through mixing enhancement. <https://www.semanticscholar.org/paper/Control-of-Jet-Noise-Through-Mixing-Enhancement-BridgesWernet/04620a13cae28f1a0cfc92914d3025b5a8f29f6a>
- Brown, G. L., & Roshko, A. (1974). On density effects and large structure in turbulent mixing layers. *Journal of Fluid Mechanics*, 64, 775 – 816. <https://doi.org/10.1017/S002211207400190X>
- Crow, S. C., & Champagne, F.H. (1971). Orderly structure in jet turbulence. *Journal of Fluid Mechanics*, 48, 547-591. <https://doi.org/10.1017/S0022112071001745>
- Dharmahinder Singh Chand, Thanigaiarasu, S., Elangovan, S., & Rathakrishnan, E. (2011). Perforated arc-tabs for jet control. *Int. J. Turbo Jet-Engines*, 28, 133-138. <https://doi.org/10.1515/tjj.2011.012>
- Jyothy, V. M., Wessley, G. J. J., & Solomon, A. B. (2023). Study of wedge-shaped Jet tabs for effective Thrust

- vector control in Supersonic vehicles. *Aerospace Systems*, 7(3), 565–573. <https://doi.org/10.1007/s42401-023-00257-y>
- Lovaraju, P., & Rathakrishnan, E. (2006). Subsonic and transonic jet control with cross-wire. *AIAA Journal*, 44(11), 2700–2705. <https://doi.org/10.2514/1.17637>
- Lovaraju, P., & Rathakrishnan, E. (2007). Effect of cross-wire location on the mixing of underexpanded sonic jets. *Journal of Aerospace Engineering*, 20(3), 179–185. [https://doi.org/10.1061/\(ASCE\)0893-1321\(2007\)20:3\(179\)](https://doi.org/10.1061/(ASCE)0893-1321(2007)20:3(179)).
- Parker, R. L., Rajagopalan, S., & Antonia, R. A. (2003). Control of an axisymmetric jet using a passive ring. *Experimental Thermal and Fluid Science*. [https://doi.org/10.1016/s0894-1777\(02\)00268-6](https://doi.org/10.1016/s0894-1777(02)00268-6)
- Richards, S. B. J., Thanigaiarasu, S., & Kaushik, M. (2023). Experimental study on the effect of tabs with asymmetric projections on the mixing characteristics of subsonic jets. *Journal of Applied Fluid Mechanics*, 16(6). <https://doi.org/10.47176/jafm.16.06.1584>
- Richards, S. B. J., Thanigaiarasu, S., Rajendran, P., & Rathakrishnan, E. (2024). An innovative vortex generator for promoting subsonic and sonic jet mixing. *Proceedings of the Institution of Mechanical Engineers Part G Journal of Aerospace Engineering*. <https://doi.org/10.1177/09544100241308966>
- Sadeghi, H., & Pollard, A. (2012). Effects of passive control rings positioned in the shear layer and potential core of a turbulent round jet. *Physics of Fluids*, 24(11). <https://doi.org/10.1063/1.4767535>
- Samimy, M., Zaman, K. B. M. Q., & Reeder, M. F. (1993). Effect of tabs on the flow and noise field of an axisymmetric jet. *AIAA Journal*, 31(4), 609–619. <https://doi.org/10.2514/3.11594>
- Thanigaiarasu, S., Balamani, G., Mirnal, K., & Revathy, K. (2023). Computational study on the effect of vane design in enhancing the mixing of subsonic jet and sonic jet. *Journal of Applied Fluid Mechanics*, 16(12). <https://doi.org/10.47176/jafm.16.12.2092>
- Thanigaiarasu, S., Jayaprakash, S., Elangovan, S., & Rathakrishnan, E. (2008). Influence of tab geometry and its orientation on under-expanded sonic jets. *Proceedings of the Institution of Mechanical Engineers, Part G: Journal of Aerospace Engineering*, 222(3), 331-339. <https://doi.org/10.1243/09544100JAERO299>
- Thanigaiarasu, S., Yadav, S. K., Jabez Richards, S. B., Muthuram, A., & Vijay Raj, T. (2020). Effects of circular tabs on enhancement of jet mixing. *Lecture Notes in Mechanical Engineering*, 433–440. [https://doi.org/10.1007/978-981-15-4756-0\\_37](https://doi.org/10.1007/978-981-15-4756-0_37)
- Tong, C., & Warhaft, Z. (1994). Turbulence suppression in a jet by means of a fine ring. *Physics of Fluids*. <https://doi.org/10.1063/1.868087>
- Venkatramanan, S., Thanigaiarasu, S., & Kaushik, M. (2024). Enhancement of jet mixing using stepped tandem tabs. *Journal of Applied Fluid Mechanics*, 17(5). <https://doi.org/10.47176/jafm.17.05.2217>
- Zaman, K. B. M. Q., Reeder, M. F., & Samimy, M. (1992). Supersonic jet mixing enhancement by delta-tabs. *AIAA*, 92, 3548, 1992. <https://doi.org/10.2514/6.1992-3548>
- Zaman, K. B. M. Q., Reeder, M. F., & Samimy, M. (1994). Control of an axisymmetric jet using vortex generators. *Physics of Fluids*, 6(2), 778-793. <https://doi.org/10.1063/1.868316>